Effect of Mesostructured Zirconia Support on the Activity and Selectivity of 4,6-Dimethydibenzothiophene Hydrodesulfurization

Sylvette Brunet [1] , **Bénédicte Lebeau** [2,3] , **Issam Naboulsi** [4] **, Laure Michelin** [2,3] **,**
Jean Dominique Comparot [1] **, Claire Marichal** [2,3] **, Séverinne Rigolet** [2,3] **, Magali Bonne** [2,3] **and**
Jean-Luc Blin [4,*]

[1] CNRS, IC2MP, UMR 7285, Université de Poitiers, 86073 Poitiers CEDEX 9, France;
sylvette.brunet@univ-poitiers.fr (S.B.); jean-dominique.comparot@univ-poitiers.fr (J.D.C.)

[2] CNRS, IS2M, UMR 7361, Université de Haute Alsace (UHA), F-68100 Mulhouse, France;
benedicte.lebeau@uha.fr (B.L.); laure.michelin@uha.fr (L.M.); Claire.Marichal@uha.fr (C.M.);
severinne.rigolet@uha.fr (S.R.); magali.bonne@uha.fr (M.B.)

[3] Université de Strasbourg, F-67000 Strasbourg, France

[4] CNRS, L2CM, Université de Lorraine, F-54000 Nancy, France; issam_naboulsi@hotmail.com

[*] Correspondence: jean-luc.blin@univ-lorraine.fr; Tel.: +33-3-83-68-43-70

Abstract: In contrast with the conventional CoMoS/alumina catalyst, the use of amorphous mesostructured ZrO_2 as support for the dispersion of the CoMoS active phase in deep hydrodesulfurization (HDS) of 4,6-dimethyldibenzothiophene led to a higher promotion rate and a better sulfidation of the cobalt species. The CoMoS, dispersed over mesostructured amorphous ZrO_2 as catalyst, also induced a modification of the main desulfurization way; in this case, a shift towards direct desulfurization selectivity was observed. This result was unexpected regarding the literature. Indeed, the hydrogenated route was observed for commercial zirconia. The designed catalysts are therefore more eco-friendly, since they consume less hydrogen. This implies a better use of the fossil resources.

1. Introduction

Because it can cause health problems (cancer, etc.), air quality in cities is a major issue; the latter is affected by atmospheric pollution to which the gas emissions from vehicles contribute in a significant way, in particular by the emission of sulfur oxides. In order to limit this impact, standards have been fixed to have fuels that are more respectful of the environment. For example, in Europe since 2009, the maximum sulfur content is limited to 10 ppm [1]. Considering the increase in consumption of fuels, in particular in emerging countries, and the diversity of the origin of the raw material (mainly from fossil material, but also from lipidic or lignocellulosic biomass in a less extent), the hydrotreatment processes have a great interest. For diesel cuts, it is admitted that 4,6-dimethydibenzothiophene (46DMDBT) is the most representative compound of the most refractory sulfated molecules [2–5]. Hydrotreating catalysis is a highly mature field, and catalyst manufacturers have improved and optimized the preparation of alumina-supported, Co- or Ni-promoted, MoS_2 catalysts over decades. However, one aspect that has been somewhat neglected in industrial development is the important role of the support. Industrial hydroprocessing catalysts are almost exclusively supported on alumina [6].

Due to the strong interaction between alumina and the support, the formation of the active phase during the sulfidation process is not optimal, especially when catalysts are promoted [7]. Different activities and selectivities can be noticed when alumina is replaced by silica, titania, or zirconia [8–13]. Indeed, since the interactions of the support with Mo will modify the electronic properties of the coordinately unsaturated sites (CUS) [14], which are well identified as the active phases, the support plays an important role in improving the properties of a catalyst in terms of activity, selectivity, and stability. For example, it has been reported that the intrinsic activity of MoS_2 deposited on titanium oxide is greater than that of MoS_2 supported on alumina [15,16]. In addition, studies performed in Raman spectroscopy and X-ray photoelectron spectroscopy (XPS) reveal that molybdate anions are strongly and uniformly bound to the surface of titanium oxide. This homogeneous dispersion is related to the distribution of hydroxyl groups at the surface of TiO_2 [17]. Shimada [18] has shown that the structure of TiO_2 facilitates the formation of MoS_2 slabs, which contribute to the increase in the catalytic activity. Ishihana et al. [19] highlighted the role of Ti^{3+}, which could have an electronic effect on the active phase. More recently, by comparison with conventional catalysts, we have shown that a change of selectivity for the hydrodesulfurization (HDS) of 46DMDBT is obtained when the active phase is dispersed on mesostructured titania [20]. This behavior has been correlated for one part of the intrinsic properties of the mesostructured titania [20].

Among the different oxides, zirconia is also of peculiar interest for hydrodesulfurization (HDS) of gazole [12,21–25]. It is reported that for the same amount of molybdenum atom per nm^2, the activity of the catalyst deposited on a zirconia support is three times higher than when it is deposited on alumina [24]. Regarding promoted catalyst by Ni, due to a better promotion on ZrO_2 than on Al_2O_3, an enhancement of the NiMoS activity is noted [25]. Another study, reported by Li et al. [23] evidenced that on a zirconia support, nickel is sulfided much more easily than on alumina, making the catalyst more efficient in term of activity [23]. Therefore, ZrO_2 appears as an interesting material for the dispersion of the active phase to prepare the HDS catalyst with high activity and selectivity [12]. However, the specific surface area of ZrO_2 ($\approx$100 m^2/g) is quite low compared to silica or γ-alumina ($\approx$250 m^2/g) and it is thermally unstable. To overcome these drawbacks zirconia is usually used in mixture with alumina or silica. Since good textural properties are considered to be the most important criteria that any catalyst support should fulfill for the hydrotreating of heavy feeds [26–28], an increase in the specific surface area of zirconia could have beneficial effects on the activity of the ZrO_2-based catalyst. Thanks to their properties, mesostructured metal oxides are excellent candidates to meet the criteria required, i.e., high specific surface area, well-ordered uniform pore structure containing mesopores stable to thermal treatments, and narrow pore size distribution, for an efficient hydrotreatment catalyst support. Recently, we have reported the preparation of mesostructured amorphous zirconia with high specific surface area (>300 m^2/g) and thermal stability (>480 °C). The ZrO_2 is obtained by combining the surfactant templating pathway and the sol–gel process from an Evaporation Induced Self Assembly-derivate method [29]. Here, due to the interest of zirconia for hydrotreatment, the mesostructured amorphous zirconia has been used as support to design MoS_2/ZrO_2 catalyst promoted by cobalt, which has been tested for the hydrodesulfurization of 46DMDBT. In particular, we have investigated the effect of the ZrO_2 on the selectivity of the catalyst. Catalytic results are compared with the ones obtained by dispersing the active phase on the conventional alumina support.

2. Results and Discussion

2.1. Characterization of the Mesostructured ZrO_2-based Catalyst

Before sulfidation was used to get to the active phase, the support was impregnated with cobalt and molybdenum precursors. At each step materials were characterized. The SAXS (small angle X-ray scattering) pattern of the bare zirconia exhibited one broad peak centered at around 8.1 nm (Figure 1a), meaning that the mesopore network adopted a wormhole-like structure analogous to the

one reported for the silica MSU (Michigan State University) materials [30], which presented a lack of long-range crystallographic order. The position of the broad peak corresponded to the sum of the pore diameter and the wall thickness. A type IV isotherm, characteristic of mesoporous material according to the IUPAC (International Union of Pure and Applied Chemistry) classification [31], was obtained by nitrogen adoption–desorption analysis (Figure 1b). The values of the specific surface area and of the pore volume were equal to 420 m^2/g and 0.43 cm^3/g, respectively. The mesopore size distribution was homogeneous, with a maximum at 4.6 nm. The wall thickness was thus around 3.5 nm. After impregnation, the wormhole-like mesostructure was preserved, as confirmed by the presence of a broad peak centered at 7.2 nm (Figure 1a). According to the broadness of the peaks, the difference in the maxima before and after impregnation was not significant, and one can conclude that the structural properties were barely influenced by the wet impregnation. The shapes of the isotherm and of the mesopore size distribution were not modified either (Figure 1b,c). However, comparing the bare ZrO$_2$, the lower quantity of adsorbed nitrogen (Figure 1b) and lower dV/dD values (Figure 1c) were noticed. These decreases could be correlated to the drop of the BET (Brunauer–Emmett–Teller) specific surface area to 255 m^2/g, pore volume to 0.25 cm^3/g, and pore diameter to 3.9 nm. The variation of textural characteristics was mainly due to the mesopores filled by the molybdenum and cobalt species. Moreover, the similitude in the shape of both N$_2$ sorption and pore size distribution shape reflected a homogeneous dispersion of Mo and Co species.

(**a**)　　　　　　　　　　(**b**)　　　　　　　　　　(**c**)
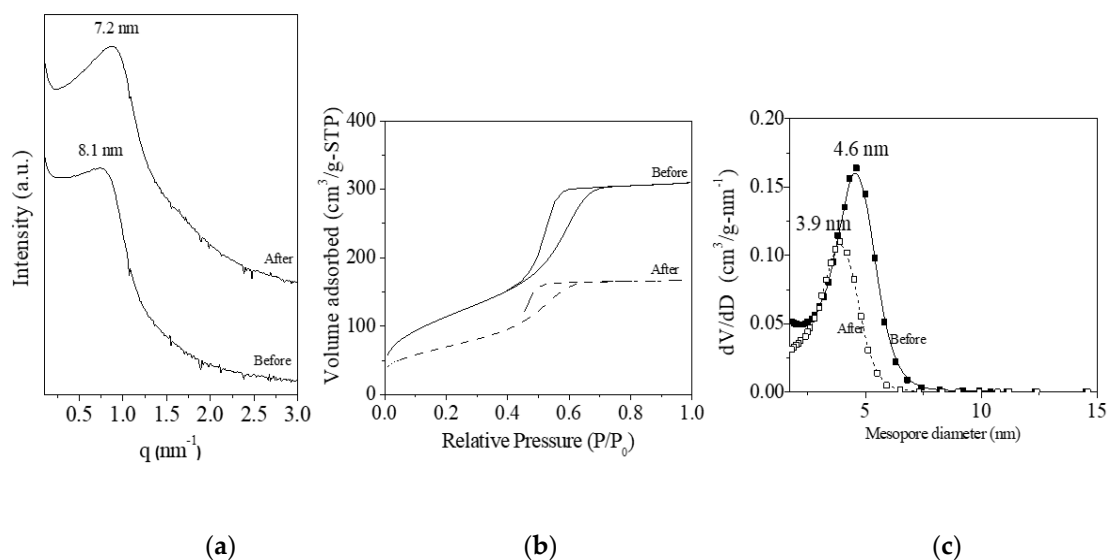
Figure 1. Small Angle X-ray Scattering (SAXS) pattern (**a**), nitrogen adsorption–desorption isotherms, (**b**) and mesopores size distribution (**c**) of the bare and of the impregnated amorphous mesostructured ZrO$_2$.

The acidity properties of the impregnated zirconia material were investigated by pyridine adsorption followed by infrared (Figure 2). Obtained spectra were in accordance with those reported in literature [32–35]. The intensities of the band at around 1540 and 1447–1452 cm^{-1} were used to quantify the Lewis and Brønsted acidity. From Figure 2, no significant Brønsted site was detected and the Lewis acidity of CoMo/ZrO$_2$ (0.90 µmol.m^{-2}) was similar to the one measured for the impregnated alumina ($\approx$1.1 µmol.m^{-2}), which will be used as the benchmark catalyst for HDS.

After sulfidation, two peaks located at 182.1 eV and 184.5 eV were observed on the XPS Zr 3d spectrum (Figure 3a). They were characteristic of ZrO$_2$ [36]. XPS also evidenced the success of the sulfidation process (Figure 3). Indeed, on the molybdenum spectrum, we could observe at 231.9 (Mo 3d$_{3/2}$) and 228.8 eV (Mo 3d$_{5/2}$), the +IV oxidation state of Mo bonded with the sulfur atoms (Figure 3b). Three peaks at 778.7, 778.0, and 780.8 eV with the associated satellites were detected on the Co 2p$_{3/2}$ spectrum. They were due to CoMoS, Co$_9$S$_8$, and CoOx, respectively [37]. The formation of the active phase was also supported by the presence of the peak S 2p$_{1/2}$ and S 2p$_{3/2}$ located around

162.7 and 161.2 eV (Figure 3d). In the sake of comparison, the impregnated commercial Al_2O_3 was sulfided under the same conditions as that of the mesostructured zirconia. No significant difference in the formation of the various phases was noted between ZrO_2 and Al_2O_3 after sulfidation (Table 1). However, the proportion of CoMoS obtained on ZrO_2 (33%) was slightly higher than the one observed on Al_2O_3 (26%), suggesting a better sulfidation of cobalt on mesostructured zirconia.
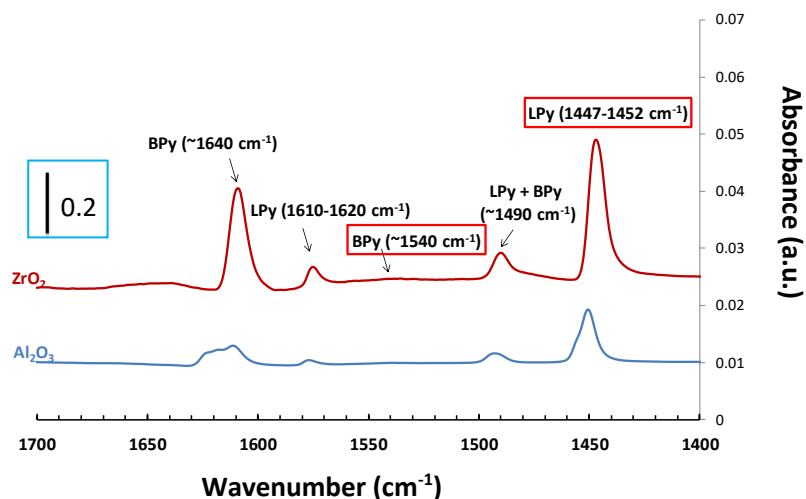

Figure 2. Infrared spectra of pyridine adsorbed on $CoMo/Al_2O_3$ and $CoMo/ZrO_2$.
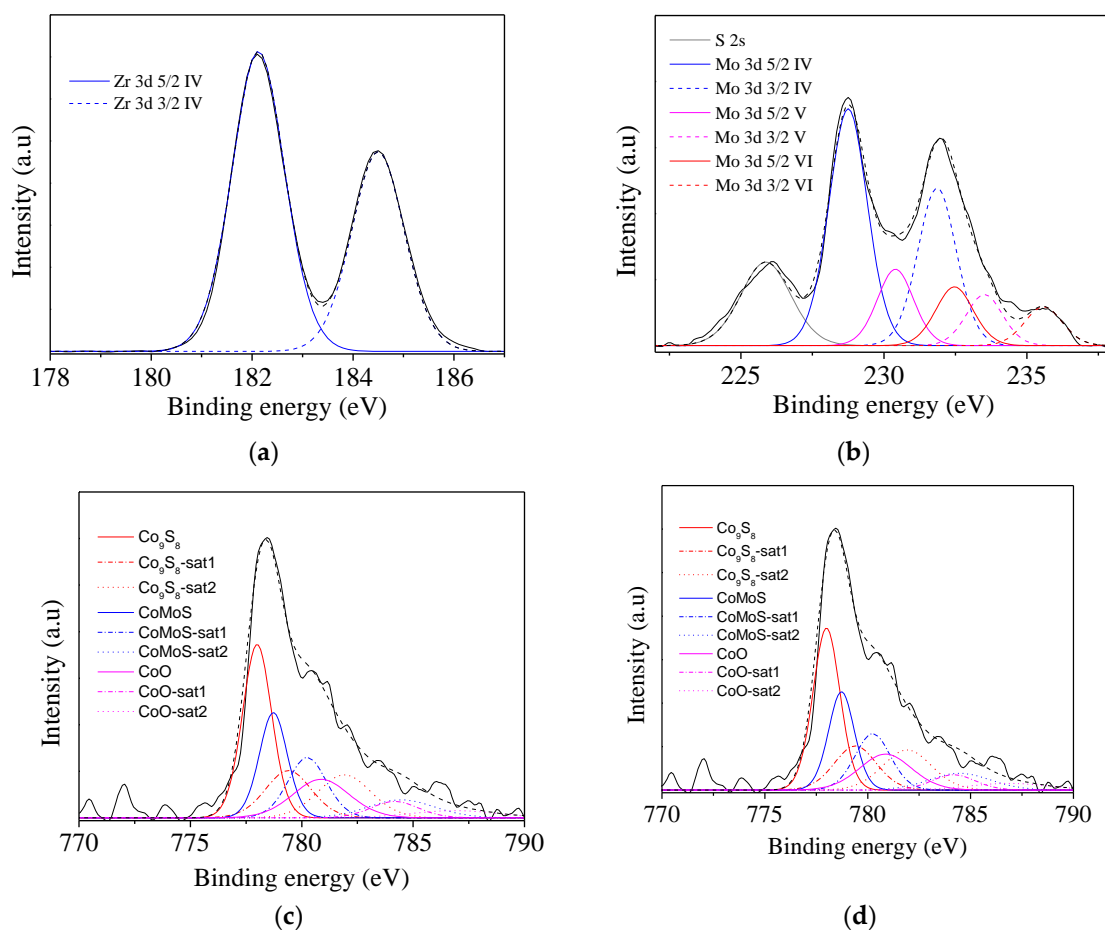

Figure 3. Zr 3d (**a**), Mo 3d (**b**), Co 2p (**c**), and S 2p (**d**) X-ray photoelectron spectroscopy (XPS) spectra of the CoMoS/ ZrO_2 catalyst.

Table 1. Percentage obtained by XPS analysis of the phases formed after sulfidation.

Oxide	Mo Distribution (at.%)			Co Distribution (at.%)			S Distribution (at.%)	
	MoS_2	Mo^{5+}	MoO_3	CoMoS	Co_9S_8	CoO	Sulfur	Sulfates
ZrO_2	65	20	16	33.0	48.7	18.3	90.7	9.3
Al_2O_3 *	70	15	15	25.7	52.3	22	100	0

* used as reference for 46DMDBT hydrodesulfurization.

From Table 1, data characterizing the active phase have been determined from the relations reported in Reference [21].

From XPS analysis, the sulfidation rate of molybdenum (TSMo), the global sulfidation degree (TSG), promotion rate (PR) and the promoter ratio [(Co/Mo)slabs] have been calculated The obtained values are given in Table 2. The sulfidation degree of Mo was similar for both supports, since the amount of MoS_2 obtained at the surface of alumina (70%) and mesostructured zirconia (65%) were very closed, suggesting that interactions between Mo and Zr were in the same range of order than the ones between Mo and Al [38]. The better sulfidation of the cobalt species on mesostructured ZrO_2 was also reflected by higher values of the promoter ratio and of the promotion rate (0.3 and 33%, respectively, against 0.1 and 26% for the alumina support).

Table 2. Parameters characterizing the active phase.

Oxide	TSMo (%)	TSG (%)	PR (%)	S/Mo	Co/Mo	(Co/Mo)$_{slabs}$
ZrO_2	65	56	33	1.6	0.6	0.3
Al_2O_3 *	70	53	26	1.5	0.3	0.1

* used as reference for 46DMDBT hydrodesulfurization.

2.2. Catalytic Activity for Hydrodesulfurization of 46DMDBT HDS

The obtained catalysts were tested for the hydrodesulfurization of 46DMDBT, which was the model molecule representative of the most refractory ones contained in gazole cuts. According to the literature [5], it is well established that the transformation of 46DMDBT converts via three pathways: the hydrogenation (HYD), the direct desulfurization (DDS), and the acidic ways (Figure 4). Acidic route was observed for catalysts such as zeolites, which presented Brønsted acid sites at their surface [39,40].

Activities of CoMoS/Al_2O_3 and of CoMoS/mesostructured ZrO_2 catalysts are given in Table 3. We can consider that the total activity was in the same range of order for both catalysts: 0.73 and 0.61 mmol.h^{-1}g^{-1} for CoMoS/Al_2O_3 and CoMoS/ZrO_2, respectively. The conventional alumina-based catalyst was highly selective (75%) for the hydrogenated route. This result was in good accordance with literature [6]. The situation was quite different when mesostructured amorphous zirconia was used as support. Indeed, in that case the contribution of the HYD pathway to the total activity fell to 41%. The direct desulfurization pathway predominated (59%). A detailed analysis of the DDS activity highlighted that the direct C–S bond rupture (green route in Figure 4) mainly contributed to the total DDS activity (85%). We noted also a slight participation (15%) of the acidic way of the blue pathway in Figure 4 (dismutation and isomerization), which was unexpected regarding the acidic properties of the CoMo impregnated ZrO_2. Indeed, as mentioned above, CoMo/ZrO_2 exhibited only Lewis acidity similar to the one of CoMo/Al_2O_3.

To explain the appearance of the desulfurization products through the dismutation and isomerization reactions, we can assume that during the sulfidation and/or HDS reaction, a part of the amorphous phase was transformed into monoclinic structure. Indeed, in a paper dealing with the surface characterization of zirconia polymorphs by infrared analysis after pyridine adsorption, Sun et al. [41] showed that Lewis acid sites were present on amorphous, monoclinic, and tetragonal ZrO_2, with a variation of their intensity in the order of amorphous ZrO_2 > monoclinic ZrO_2 > tetragonal ZrO_2. By contrast, using this probe, Brønsted sites were detected only for the monoclinic zirconia. Tao et al. [42] also reported similar conclusions in a study concerning a comparison of the surface acidic

properties of tetragonal and monoclinic nanostructured zirconia. Moreover, a higher amount of Lewis acid sites was obtained for the monoclinic ZrO_2 [43].
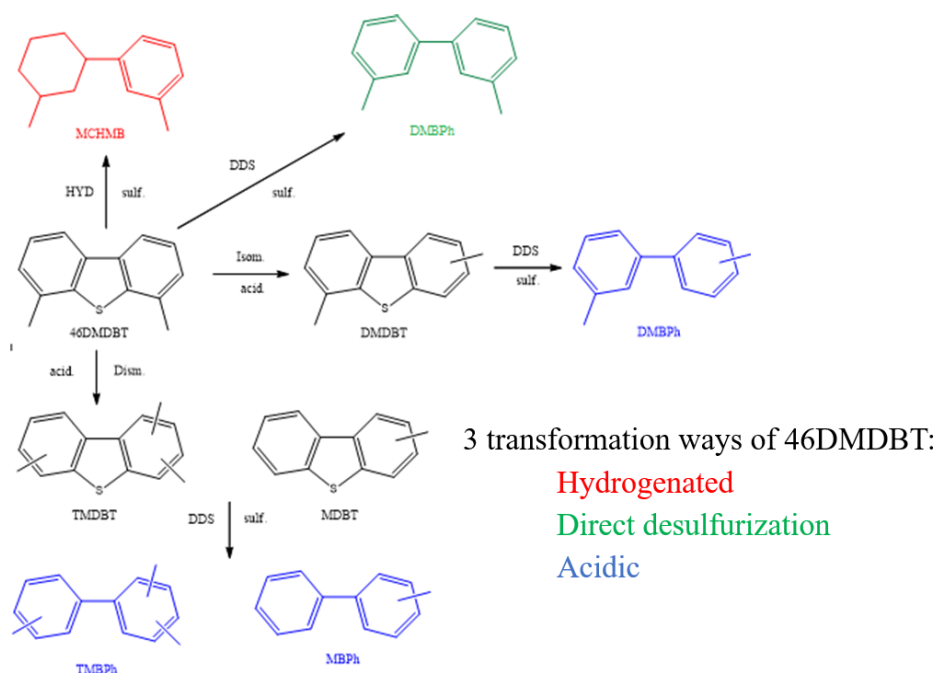
Figure 4. Transformation ways of 46DMDBT (HYD: hydrogenation route, DDS: direct desulfurization route, sulf: sulfide phase, acid: acid properties, dism: dismutation, isom: isomerization. 4,6-DMDBT: 4,6-dimethyldibenzothiophene, MCHMB: methylcyclohexylmethylbenzene, MBPh: methylbiphenyl, DMDBT: dimethyldibenzothiophene, DMBPh: dimethylbiphenyl, TMDBT: trimethylbiphenyl, MBPh: methylbiphenyl).

Table 3. The 46DMDBT HDS activities (A mmol.h^{-1}.g^{-1}) and selectivity (%) obtained for CoMoS/Al$_2$O$_3$ and CoMoS/ZrO$_2$ materials (T = 340 °C, P = 40 bars, H$_2$/feed = 475 NL/L).

Materials	A_{total}	A_{acid}	A_{HYD}	$A_{total\ DDS}$	A_{HYD}/A_{DDS}
CoMoS/Al$_2$O$_3$	0.73	0.00	0.55(75%)	0.18(25%)	3.1
CoMoS/ZrO$_2$	0.61	0.17	0.18(41%)	0.26(59%)	0.7

A_{total}: represents the total activity. A_{acid}, A_{HYD}, and $A_{total\ DDS}$ stand for the activity obtained from the acidic, the hydrogenated and the direct desulfurization routes, respectively.

The inversion of selectivity observed for the CoMoS/ZrO$_2$ catalyst was quite unexpected regarding the literature. For example, for HDS of 46DMDBT, Ninh et al. [44] obtained a HYD/DDS ratio of 1.43 and 0.60 for CoMoS dispersed on ZrO$_2$ and Al$_2$O$_3$, respectively. In their study, the authors used a commercial monoclinic ZrO$_2$ (S_{BET} = 96 m^2/g) as support. Orosco et al. reported that the HYD activity of MoS$_2$ deposited on ZrO$_2$, was twice the one of MoS$_2$ dispersed on Al$_2$O$_3$ [22]. In our case, even if the acidic route contributed to the DDS pathway, the change of selectivity cannot be explained only by this contribution. Indeed, in that case, the main contribution arose from the direct cleavage of the C–S bond. From Table 4, it can be seen that for the zirconia-based catalyst, the activity per m^2 is lower. This could be expected since the amorphous ZrO$_2$ had a higher specific surface area than Al$_2$O$_3$. However, the same tendency was noted for the activity per atom of Mo; we can thus assume that the difference in activity and selectivity may have been due to a modification of the active sites which are the molybdenum atoms. This involved different interactions with the support because of the presence of the amorphous phase, which will lead to modifications of the electronic properties, as already observed with TiO$_2$ [20]. Indeed, in a recent study [29], we showed that the prepared amorphous mesostructured ZrO$_2$ exhibited a high thermal stability up to 400 °C. We can thus assume

that the change in selectivity was mainly due to the presence of this amorphous phase, which likely modified the intermediates of reaction by favoring the ones involved in the direct rupture of the C–S bond [5], and/or by modifying the properties of the active phase.

Table 4. The 46DMDBT HDS activities (A): (a: (mmol.h^{-1}.m^{-2}). 10^{-3}); (b (mmol.h^{-1}.Mo atom^{-1}).10^{-21}) for CoMoS/Al$_2$O$_3$ and CoMoS/ZrO$_2$ materials (T = 340 °C, P = 40 bars, H$_2$/feed = 475 NL/L).

Materials	A$_{total}$		A$_{acid}$		A$_{HYD}$		A$_{total\ DDS}$	
	(a)	(b)	(a)	(b)	(a)	(b)	(a)	(b)
CoMoS/Al$_2$O$_3$	6	2	0	0	4.5	0.5	1.5	0.5
CoMoS/ZrO$_2$	2.5	0.9	0.68	0.3	0.72	0.2	1.1	0.4

A$_{total}$: represents the total activity. A$_{acid}$, A$_{HYD}$, and A$_{total\ DDS}$ stand for the activity obtained from the acidic, the hydrogenated and the direct desulfurization routes, respectively.

3. Materials and Methods

3.1. Materials Preparation

Amorphous mesostructured ZrO$_2$ was prepared according the procedure described in reference [29]. The wet impregnation used CoN$_2$O$_6$, 6H$_2$O, 99.00% Si (Sigma-Aldrich Chemie S.a.r.l., Saint-Quentin Fallavier, France) and (NH$_4$)$_6$Mo$_7$, 6H$_2$O, 99.98% (Sigma-Aldrich Chemie S.a.r.l., Saint-Quentin Fallavier, France) precursors and was performed under the same conditions as the ones reported in Reference [20].

As reported in previous papers [20], the catalyst was sulfided in situ before the catalytic reaction, in the presence of hydrogen by the hydrogen sulfide, resulting from the decomposition of dimethyl disulfide (DMDS). The sulfurizing charge consisted of a mixture of n-heptane and DMDS (5 by weight). The sulfurizing feed and hydrogen flow rates were respectively 8 mL/h and 4.7 L/h for an H$_2$/feed ratio of 587 NL/L. The sulfurizing charge was injected at 150 °C. After 1 h of sulfidation at 150 °C, the temperature was raised to 350 °C at a rate of 5 °C/min, then maintained at 350 °C for 14 h. After this plateau, the temperature was lowered to 340 °C.

3.2. Characterization

SAXS measurements were carried out using on a SAXSess mc^2 (Anton Paar, Vienna, Austria), equipped with a classical tube (λ Cu, Kα = 0.1542 nm) operating at 40 kV and 50 mA. Textural properties were evaluated from TRISTAR 3000 sorptometer (Micromeritics, Merignac, France). The BET and the BJH (Barrett, Joyner, Halenda) equations were applied to determine the specific surface areas and the repartition of the mesopores diameters.

XPS spectra were collected on a Kratos Axis Ultra (Kratos Analytical, Manchester, United Kingdom) spectrometer with a hemispherical energy analyzer, using a monochromatic Al Kα source (1486.6 eV). The peak at 284.6 eV was taken as reference for the bending energies.

3.3. Catalytic Tests

The transformation of 4.6DMDBT was studied under HDS conditions of a diesel cut at a temperature of 340 °C under a total pressure of 4.0 MPa, while maintaining the H$_2$/HC ratio constant and equal to 475 NL/L. The model charge, containing 1% by weight of sulfur, consisted of 500 ppm S from (4.6DMDBT) and 9500 ppm S of H$_2$S generated by dimethyl disulfide (DMDS) diluted in n-heptane. The transformation of 46DMDBT was measured for a conversion of 25%, which corresponded to liquid feed and hydrogen flow rates of 48 mL/h and 22.8 L/h, respectively, while keeping the H$_2$/HC ratio constant (equal to 475 NL/L). Organic products were analyzed by gas chromatography (Varian 3400 GC, Agilent, Paris, France), using a flame ionization detector (FID). The different products were separated on a non-polar Durabond (D B 1) type capillary column (Agilent, Paris, France), 30 min length, with an internal diameter of 0.32 mm and a film thickness of 5 μm. The experiment conditions

were as follows: a plateau of 30 s at 50 °C, followed by a rise in temperature at 2 °C/min up to 60 °C, then at 7 °C/min to end at a temperature of 250 °C, which was maintained for 18 min. The temperatures of the injector and the detector were set at 320 °C. The samples taken over time were injected (2 μL) into the chromatograph using a micro-syringe.

4. Conclusions

Mesostructured amorphous ZrO_2 were wet impregnated and sulfided to prepare the catalyst for the 46DMDBT hydrodesulfurization.

Comparing the conventional alumina support, a higher promotion rate and an enhancement of the sulfidation of Co species was observed.

Compared to CoMoS supported over conventional Al_2O_3, a similar total activity was measured, but the direct desulfurization pathway predominated over the hydrogenated route when amorphous mesostructured zirconia was used as support. This result was unexpected since according to literature, commercial zirconia favors the hydrogenated route. This study emphasized the role of the amorphous phase on the selectivity.

Author Contributions: I.N.: investigation; L.M.: investigation; J.D.C.: investigation; S.R.: investigation; M.B.: investigation; C.M.: formal analysis; S.B.: resources, formal analysis; B.L.: resources, supervision; J.-L.B.: writing—original draft, supervision. All authors have read and agreed to the published version of the manuscript.

Conflicts of Interest: The authors declare that they have no competing interests.

References

1. EU: Fuels: Diesel and Gasoline. Available online: https://www.transportpolicy.net/standard/eu-fuels-diesel-and-gasoline (accessed on 24 August 2020).
2. Whitehurst, D.D.; Isoda, T.; Mochida, I. Present state of the art and future challenges in the hydrodesulfurization of polyaromatic sulfur compounds. *Adv. Catal.* **1998**, *42*, 345–471.
3. Landau, M.V. Deep hydrotreating of middle distillates from crude and shale oils. *Catal. Today* **1997**, *36*, 393–429. [CrossRef]
4. Ma, X.; Sakanishi, K.; Mochida, I. Hydrodesulfurization reactivities of various sulfur compounds in vacuum gas oil. *Ind. Eng. Chem. Res.* **1996**, *35*, 2487–2494. [CrossRef]
5. Bataille, F.; Lemberton, J.L.; Michaud, P.; Pérot, G.; Vrinat, M.; Lemaire, M.; Schulz, E.; Breysse, M.; Kasztelan, S. Alkyldibenzothiophenes hydrodesulfurization-promoter effect, reactivity, and reaction mechanism. *J. Catal.* **2000**, *191*, 409–422. [CrossRef]
6. Bej, S.K.; Maity, S.K.; Turaga, U.T. Search for an efficient 4,6-DMDBT hydrodesulfurization catalyst: A review of recent studies. *Energy Fuels* **2004**, *5*, 1227–1237. [CrossRef]
7. Stanislaus, A.; Marafi, A.; Rana, M.S. Recent advances in the science and technology of ultra low sulfur diesel (ULSD) production. *Catal. Today* **2010**, *153*, 1–68. [CrossRef]
8. Sundaramurthy, V.; Eswaramoorthi, I.; Dalai, A.K.; Adjaye, J. Hydrotreating of gas oil on SBA-15 supported NiMo catalysts. *Microporous Mesoporous Mater.* **2008**, *111*, 560–568. [CrossRef]
9. Klimova, T.; Peña, L.; Lizama, L.; Salcedo, C.; Gutiérrez, O.Y. Modification of activity and selectivity of NiMo/SBA-15 HDS catalysts by grafting of different metal oxides on the support surface. *Ind. Eng. Chem. Res.* **2009**, *48*, 1126–1133. [CrossRef]
10. Duchet, J.C.; Tilliette, M.J.; Cornet, D.; Vivier, L.; Perot, G.; Bekakra, L.; Moreau, C.; Szabo, G. Catalytic properties of nickel molybdenum sulphide supported on zirconia. *Catal. Today* **1991**, *10*, 579–592. [CrossRef]
11. Kumaran, G.M.; Garg, S.; Soni, K.; Prasad, V.V.D.N.; Sharma, L.D.; Murali Dhar, G. Catalytic functionalities of H-β-zeolite-supported molybdenum hydrotreating catalysts. *Energy Fuels* **2006**, *20*, 1784–1790. [CrossRef]
12. Breysse, M.; Afanasiev, P.; Geantet, C.; Vrinat, M. Overview of support effects in hydrotreating catalysts. *Catal. Today* **2003**, *86*, 5–16. [CrossRef]

13. Prabhu, N.; Dalai, A.K.; Adjaye, J. Hydrodesulphurization and hydrodenitrogenation of light gas oil using NiMo catalyst supported on functionalized mesoporous carbon. *Appl. Catal. A Gen.* **2011**, *401*, 1–11. [CrossRef]

14. Ramireza, J.; Macıas, G.; Cedenoa, L.; Gutierrez-Alejandre, A.; Cuevasa, R.; Castillo, P. The role of titania in supported Mo, CoMo, NiMo, and NiW hydrodesulfurization catalysts: Analysis of past and new evidences. *Catal. Today* **2004**, *98*, 19–30. [CrossRef]

15. Platanitisa, P.; Panagiotoua, G.D.; Bourikasb, K.; Kordulisa, C.; Fierrod, J.L.G.; Lycourghiotis, A. Preparation of un-promoted molybdenum HDS catalysts supported on titania by equilibrium deposition filtration: Optimization of the preparative parameters and investigation of the promoting action of titania. *J. Mol. Catal. A Chem.* **2016**, *412*, 1–12. [CrossRef]

16. Castillo-Villalón, P.; Ramírez, J.; Cuevas, R.; Vázquez, P.; Castañeda, R. Influence of the support on the catalytic performance of Mo, CoMo, and NiMo catalysts supported on Al_2O_3 and TiO_2 during the HDS of thiophene, dibenzothiophene, or 4,6-dimethyldibenzothiophene. *Catal. Today* **2016**, *259*, 140–149. [CrossRef]

17. Shimada, H.; Sato, T.; Yoshimura, Y.; Hiraishi, J.; Nishijima, A. Support effect on the catalytic activity and properties of sulfided molybdenum catalysts. *J. Catal.* **1988**, *110*, 275–284. [CrossRef]

18. Shimada, H. Morphology and orientation of MoS_2 clusters on Al_3 and TiO_2 supports and their effect on catalytic performance. *Catal. Today* **2003**, *86*, 17–29. [CrossRef]

19. Wang, D.; Qian, W.; Ishihara, A.; Kabe, T. Elucidation of Sulfidation State and Hydrodesulfurization Mechanism on TiO_2 Catalysts Using ^{35}S Radioisotope Tracer Methods. *J. Catal.* **2001**, *203*, 322–328. [CrossRef]

20. Roy, T.; Rousseau, J.; Daudin, A.; Pirngruber, G.; Lebeau, B.; Blin, J.L.; Brunet, S. Deep hydrodesulfurization of 4,6-dimethydibenzothiophene over $CoMoS/TiO_2$ catalysts: Impact of the TiO_2 treatment. *Catal. Today* **2020**. [CrossRef]

21. Mazurelle, J.; Lamonier, C.; Lancelot, C.; Payen, E.; Pichon, C.; Guillaume, D. Use of the cobalt salt of the heteropolyanion $[Co_2Mo_{10}O_{38}H_4]^{6-}$ for the preparation of CoMo HDS catalysts supported on Al_2O_3, TiO_2 and ZrO_2. *Catal. Today* **2008**, *130*, 41–49. [CrossRef]

22. Orozco, E.O.; Vrinat, M. Kinetics of dibenzothiophene hydrodesulfurization over MoS_2 supported catalysts: Modelization of the H_2S partial pressure effect. *Appl. Catal. A Gen.* **1998**, *170*, 195–206. [CrossRef]

23. Ji, Y.; Afanasiev, P.; Vrinat, M.; Li, W.; Li, C. Promoting effects in hydrogenation and hydrodesulfurization reactions on the zirconia and titania supported catalysts. *Appl. Catal. A Gen.* **2004**, *257*, 157–164. [CrossRef]

24. Breysse, M.; Portefaix, J.L.; Vrinat, M. Support effects on hydrotreating catalysts. *Catal. Today* **1991**, *10*, 489–505. [CrossRef]

25. Hamon, D.; Vrinat, M.; Breysse, M.; Durand, B.; Beauchesne, F.; Des Courieres, T. Surface structure and catalytic activities of Mo/ZrO_2-Y_2O_3 catalysts. *Bull. Soc. Chim. Belg.* **1991**, *100*, 933–943. [CrossRef]

26. Grange, P.; Vanhaeren, X. Hydrotreating catalysts, an old story with new challenges. *Catal. Today* **1997**, *4*, 375–391. [CrossRef]

27. Ancheyta, J.; Speight, J.G. *Hydroprocessing of Heavy Oil and Residua*; CRC Press; Taylor and Francis Group: Boca Raton, FL, USA, 2007.

28. Furimsky, E. Catalyst for Upgrading Heavy Petroleum Feeds. *Stud. Surf. Sci. Catal.* **2007**, *169*, 1–387.

29. Lebeau, B.; Naboulsi, I.; Michelin, L.; Marichal, C.; Rigolet, S.; Carteret, C.; Brunet, S.; Bonne, M.; Blin, J.L. Amorphous Mesostructured Zirconia with High (Hydro)Thermal Stability. *Rsc Adv.* **2020**, *10*, 26165–26176. [CrossRef]

30. Bagshaw, S.A.; Prouzet, E.; Pinnavaia, T.J. Templating of mesoporous molecular sieves by nonionic polyethylene oxide surfactants. *Science* **1995**, *269*, 1242–1244. [CrossRef]

31. Sing, K.S.W.; Everett, D.H.; Haul, R.A.W.; Moscou, L.; Pierotti, R.A.; Rouquerol, J.; Siemieniewska, T. Reporting physisorption data for gas/solid systems with special reference to the determination of surface area and porosity (Recommendations 1984), IUPAC. *Pure Appl. Chem.* **1985**, *57*, 603–619. [CrossRef]

32. Lavalley, J.C.; Anquetil, R.; Czyziewska, J.; Ziolek, M. Use of pyridine as a probe for the determination, by IR spectroscopy, of the Brønsted acid strength of M^IHNaY zeolites. *J. Chem. Soc. Trans.* **1996**, *92*, 1263–1266. [CrossRef]

33. Soni, K.K.; Mouli, K.C.; Dalai, A.K.; Adjaye, J. Effect of Ti loading on the HDS and HDN activity of KLGO on NiMo/TiSBA-15 catalysts. *Microporous Mesoporous Mater.* **2012**, *152*, 224–234. [CrossRef]

34. Du, P.; Zheng, P.; Song, S.; Wang, X.; Zhang, M.; Chi, K.; Xu, C.; Duan, A.; Zhao, Z. Synthesis of a novel micro/mesoporous composite material Beta-FDU-12 and its hydro-upgrading performance for FCC gasoline. *RSC Adv.* **2016**, *6*, 1018–1026. [CrossRef]

35. Zakharova, M.V.; Kleitz, F.; Fontaine, F.G. Lewis acidity quantification and catalytic activity of Ti, Zr and Al-supported mesoporous silica. *Dalton Trans.* **2017**, *46*, 3864–3876. [CrossRef] [PubMed]

36. Marakatti, V.; Marappa, S.; Gaigneaux, E.M. Sulfated zirconia: An efficient catalyst for the Friedel-Crafts monoalkylation of resorcinol with methyl tertiary butyl ether to 4-tertiary butylresorcinol. *N. J. Chem.* **2019**, *43*, 7733–7742. [CrossRef]

37. Bui, V.N.; Laurenti, D.; Delichère, P.; Geantet, C. Hydrodeoxygenation of guaiacol Part II: Support effect for CoMoS catalysts on HDO activity and selectivity. *Appl. Catal. B* **2011**, *101*, 246–255. [CrossRef]

38. Han, W.; Yuan, P.; Fan, Y.; Shi, G.; Liu, H.; Bai, D.; Bao, X. Preparation of supported hydrodesulfurization catalysts with enhanced performance using Mo-based inorganic–organic hybrid nanocrystals as a superior precursor. *J. Mater. Chem.* **2012**, *22*, 25340–25353. [CrossRef]

39. Farag, H.; Mochida, I.; Sakanishi, K. Fundamental comparison studies on hydrodesulfurization of dibenzothiophenes over CoMo-based carbon and alumina catalysts. *Appl. Catal. A Gen.* **2000**, *194–195*, 147–157. [CrossRef]

40. Zhou, W.; Zhou, Y.; Wei, Q.; DU, L.; Ding, S.; Jiang, S.; Zhang, Y.; Zhang, Q. Gallium modified HUSY zeolite as an effective co-support for NiMo hydrodesulfurization catalyst and the catalyst's high isomerization selectivity. *Chem. Eur. J.* **2017**, *23*, 9369–9382. [CrossRef]

41. Ma, Z.Y.; Yang, C.; Wei, W.; Li, W.H.; Sun, Y.H. Surface properties and CO adsorption on zirconia polymorphs. *J. Mol. Catal. A Chem.* **2005**, *227*, 119–124. [CrossRef]

42. Zhao, Y.; Li, W.; Zhang, M.; Tao, K. A comparison of surface acidic features between tetragonal and monoclinic nanostructured zirconia. *Catal. Commun.* **2002**, *3*, 239–245. [CrossRef]

43. Liu, C.; Wang, W.; Xu, Y.; Li, Z.; Wang, B.; Ma, X. Effect of zirconia morphology on sulfur-resistant methanation performance of MoO_3/ZrO_2 catalyst. *Appl. Surf. Sci.* **2018**, *441*, 482–490. [CrossRef]

44. Ninh, T.K.T.; Laurenti, D.; Leclerc, E.; Vrinat, M. Support effect for CoMoS and CoNiMoS hydrodesulfurization catalysts prepared by controlled method. *Appl. Catal. A Gen.* **2014**, *487*, 210–218. [CrossRef]